DOI: 10.1002/asia.201000720

Two-Photon Probes for Zn^{2+} Ions with Various Dissociation Constants. Detection of Zn^{2+} Ions in Live Cells and Tissues by Two-Photon Microscopy

Isravel Antony Danish, Chang Su Lim, Yu Shun Tian, Ji Hee Han, Min Young Kang, and Bong Rae Cho*[a]

Abstract: A series of Zn^{2+}-selective two-photon fluorescent probes (AZn-M1–AZnN) that had a wide range of dissociation constants (K_d^{TP} = 8 nM-12 μM) were synthesized. These probes showed appreciable water solubility (>3 μM), cell permeability, high photostability, pH insensitivity at pH > 7, significant two-photon action cross-sections (86–110 GM) upon complexation with Zn^{2+}, and can detect the Zn^{2+} ions in HeLa cells and in living tissue slices of rat hippocampal at a depth of >80 μm without mistargeting and photobleaching problems. These probes can potentially find application in the detection of various amounts of Zn^{2+} ions in live cells and intact tissues.

Keywords: fluorescence · fluorescent probes · live tissue · two-photon microscopy · zinc

Introduction

Zinc ion is the second-most-abundant d-block metal ion in the human brain and is an active component in enzymes and proteins.[1,2] It plays crucial roles in the survival, growth, and metabolism of unicellular and multicellular organisms. In mammalian cells, the majority of zinc ions are stored in vesicles, and the zinc-ion concentration in the cytoplasm is approximately 1 nM. The Zn^{2+}-ion homeostasis is maintained by the import of Zn^{2+} ions from—and export to—the extracellular cellular space, the endoplasmic reticulum, and intracellular vesicles. In the brain, a few millimoles of Zn^{2+} ion are stored in the presynaptic vesicles of specific types of neurons. The ions are released upon synaptic activation, are involved in the regulation of the excitatory neurotransmission, and are associated with neuronal disorders.[2] To understand the role of Zn^{2+} ions in physiology, it is crucial to visualize their distribution and transport in live cells and intact tissues. For this purpose, a variety of one-photon fluorescent (OPF) probes derived from quinoline (TSQ, Zinquin and TFLZn, QZ1 and QZ2) and fluorescein (FluoZn-3, Znpyr, ZnAF) have been developed.[3–7] However, the use of these probes with one-photon microscopy (OPM) requires relatively short excitation wavelengths (<500 nm), which limit their applications in tissue imaging owing to the shallow penetration depth (<100 μm), photobleaching, and cellular autofluorescence.

Two-photon microscopy (TPM) is an ideal tool to overcome these problems because it utilizes two photons of lower energy for the excitation. Combined with an appropriate two-photon (TP) probe, TPM can image intact tissue for a long period of time with minimum interference from artifacts of tissue preparation that can extend more than 70 μm into the tissue slice.[8] Recently, we reported TP probes for Zn^{2+} ions (AZn1 and AZn2)[9] with dissociation constants of 1.1 ± 0.1 and 0.50 ± 0.04 nM, respectively. Those probes were able to detect intracellular free Zn^{2+} ($[Zn^{2+}]_i$) in the nanomolar range in the living tissues at tissue depths ranging from 80-170 μm without interference from other metal ions and from the membrane-bound probes. To detect [Zn^{2+}] over a wide range of concentrations in the live cells and intact tissues,[10] there is a strong need for the development of TP probes with various affinities for Zn^{2+} ions.

To address this need, we have developed a series of TP probes for Zn^{2+} ions derived from 2-acetyl-6-(dimethylamino)naphthalene (acedan) as the reporter and *N,N*-di-(2-picolyl)ethylenediamine (DPEN) derivatives as Zn^{2+} ion receptors by considering the following requirements: 1) a significant TP cross-section for a bright TPM image; 2) an appreciable water solubility to stain the cells; 3) high selectivity

[a] Dr. I. A. Danish,[+] C. S. Lim,[+] Dr. Y. S. Tian, J. H. Han, M. Y. Kang, Prof. Dr. B. R. Cho
Department of Chemistry
Research Institute for Natural Sciences
Korea University, 1-Anamdong, Seoul 136-701 (Korea)
Fax: (+82) 2-3290-3121
E-mail: chobr@korea.ac.kr

[+] These two authors contributed equally to this work.

Supporting information for this article is available on the WWW under http://dx.doi.org/10.1002/asia.201000720.

and a wide range of affinity for Zn^{2+} ions; 4) large spectral shifts in different environments for the selective detection of $[Zn^{2+}]_i$ ions in the cytoplasm; 5) pH resistance; and 6) high photostability (Scheme 2). We adopted acedan from our previous work on various TP probes[11] and DPEN derivatives from the works of Nagano and co-workers[6] and Lippard and co-workers.[7] Herein, we present a series of TP fluorescent probes for Zn^{2+} ions that can detect the distribution of Zn^{2+} ions in living HeLa cells and fresh hippocampal slices at a depth of >80 μm without the problems of mistargeting and photobleaching (Scheme 1).

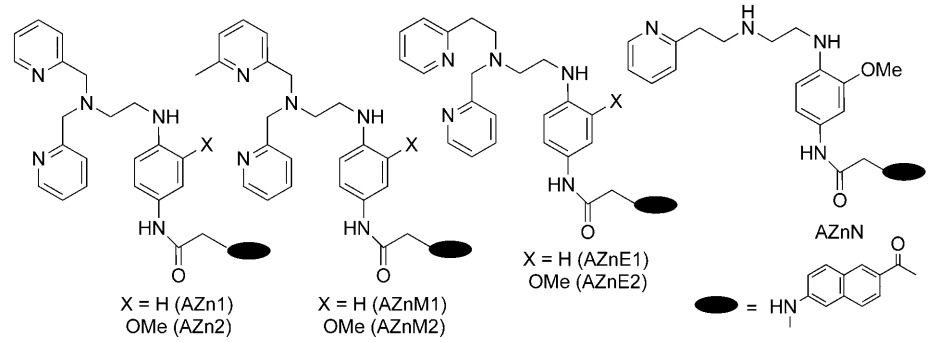

Scheme 1. Structures of AZn1–AZnN.

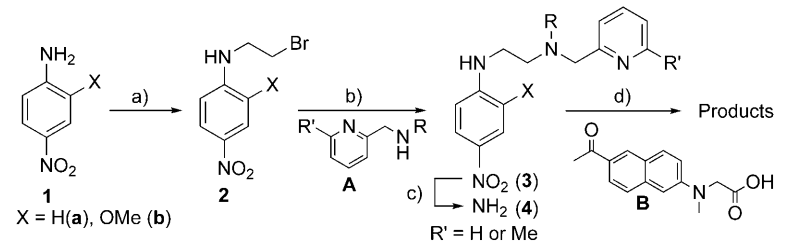

Scheme 2. Synthesis of AZM1–AZnN. a) i) 2-bromoethanol, $CaCO_3$, H_2O; ii) CBr_4, PPh_3, THF; b) **A**, K_2CO_3, KI, MeCN; c) H_2/Pd/C, EtOH; d) DCC, HOBt, **B**, CH_2Cl_2. THF = tetrahydrofuran, DCC = *N,N'*-dicyclohexylcarbodiimide, HOBt = 1-hydroxybenzotriazole.

Results and Discussion

The synthesis of AZnM1–AZnN is summarized in Scheme 2. Compound **2a** was prepared according to a literature procedure.[6b] Compound **2b** was obtained in 67% yield by the reaction of **1b** with 2-bromoethanol followed by the bromination. Substitution of the bromide (**2a,b**) with the receptor moieties (**A**) afforded **3** in yields ranging from 30–59%. Reduction of **3** to **4** proceeded in 82–95% yields. AZnM1–AZnN were obtained by the DCC coupling of **4** with **B** in 35–79% yields. All products were unambiguously characterized by ^1H and ^{13}C NMR and HRMS (see the Supporting Information).

The absorption spectra of AZnM1–AZnN were almost identical and showed gradual bathochromic shifts ($\Delta\lambda^{(1)}_{max} = 20$ nm) with the solvent polarity (E^N_T)[12] in the order 1,4-dioxane < *N,N*-dimethylformamide < ethanol < water. The fluorescence spectra showed much-larger bathochromic shifts ($\Delta\lambda^{fl}_{max} = 70$ nm) with the same variations of the solvent (see the Supporting Information, Table S1), thus confirming the utility of these molecules as polarity probes. In addition, AZnM1–AZnN was soluble in water at concentrations of up to 3.0–5.0 μM, which was sufficient to stain the cells.

When small increments of Zn^{2+} ions were added to a solution of AZnM1–AZnN in MOPS buffer (30 mM, pH 7.3, $I = 0.10$), the one- and two-photon excited fluorescence intensity increased without affecting the absorption spectra (see Figure 1 and the Supporting Information, Figure S1). This outcome can be attributed to blocking of the photo-induced electron transfer (PET) process upon complexation with Zn^{2+} ions. The fluorescence enhancement factors [$FEF = (F - F_{min})/F_{min}$] of AZn1–AZnN measured for the one- and two-photon processes ranged from 4.0–54 (Table 1). The *FEF* value was always larger for probes with a MeO group in the receptor moieties (12–54 vs 4.2–24) as a consequence of the lower fluorescence quantum yield (Φ) in the absence of Zn^{2+} ions, and the correspondingly higher Φ in the presence of excess Zn^{2+} ions (Table 1). This observation has been attributed to the dual roles of the electron-donating MeO group. The methoxy moiety elevates the HOMO level of the receptor, rendering the PET more efficient and reduces the Φ value of the probes. In addition, the tighter complexation induced by the MeO functionality also reduces the vibrational relaxation pathways and enhances the Φ value of the complexes.[9]

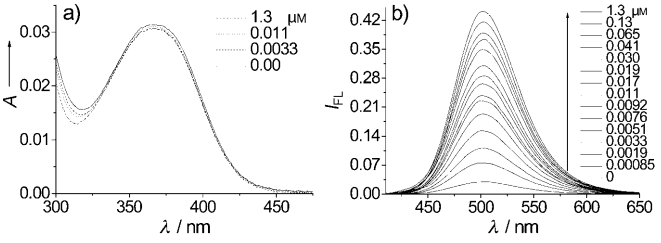

Figure 1. One-photon absorption (a) and emission (b) spectra of 1 μM AZnM2 in MOPS buffer solution (30 mM, 100 mM KCl, 10 mM NTA, pH 7.3) in the presence of free Zn^{2+} ions (0–1.3 μM). NTA = nitrilotriacetic acid.

Table 1. Photophysical data for AZnM1–AZnN.

Compound[a]	$\lambda_{max}^{(1)}/\lambda_{max}^{fl}$ [b]	Φ[c]	K_d^{OP}/K_d^{TP} [d,e]	$\lambda_{max}^{(2)}$ [f]	$\delta\Phi$[g]
AZn1[h,i]	365/496	0.02	1.1/1.1 nM	n.d.	n.d.
AZn1+Zn^{2+}	365/498	0.47		780	86
AZn2[h,i]	365/494	0.01	0.5/0.5 nM	n.d.	n.d.
AZn2+Zn^{2+}	365/499	0.65		780	95
AZnM1[i]	368/501	0.017	15/16 nM	n.d.	n.d.
AZnM1+Zn^{2+}	367/504	0.37		780	88
AZnM2[i]	364/504	0.015	8.4/7.1 nM	n.d.	n.d.
AZnM2+Zn^{2+}	363/504	0.42		780	110
AZnE1[i]	365/502	0.080	0.48/0.41 μM	n.d.	n.d.
AZnE1+Zn^{2+}	366/503	0.54		780	86
AZnE2[i]	366/503	0.026	23/21 nM	n.d.	n.d.
AZnE2+Zn^{2+}	364/504	0.39		780	86
AZnN[i]	365/500	0.018	10/12 μM	n.d.	n.d.
AZnN+Zn^{2+}	365/502	0.29		780	89

[a] Data were measured in MOPS buffer solution (30 mM, 100 mM KCl, pH 7.3) containing free Zn^{2+} ions (0–196 μM) and 10 mM NTA unless otherwise noted. [b] λ_{max} of the one-photon absorption and emission spectra in nm. [c] Fluorescence quantum yield, ±10%. [d] Dissociation constants for Zn^{2+} ions measured by one- (K_d^{OP}) and two-photon (K_d^{TP}) processes, ±14%. [e] The K_d^i values measured by the two-photon process were 9.8 nM (AZnM1), 8.7 nM (AZnM2), 0.50 μM (AZnE1), 18 nM (AZnE2), and 9.5 μM (AZnN), respectively. [f] λ_{max} of the two-photon excitation spectra in nm. [g] Two-photon action cross-section in GM. [h] Reference [[16c]]. [i] Fluorescence-enhancement factor, $(F-F_{min})/F_{min}$, measured by one-/two-photon (FEF^{op}/FEF^{TP}) processes, were 21/24 (AZn1), 54/52 (AZn2), 21/22 (AZnM1), 15/14 (AZnM2), 4.2/4.0 (AZnE1), 17/15 (AZnE2), 12/11 (AZnN), respectively.

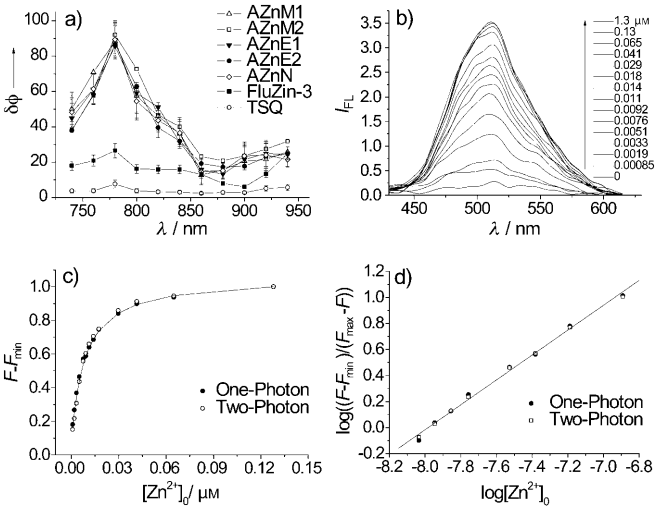

Figure 2. a) Two-photon action spectra of 1 μM AZnM1–AZnN in the presence of 1.3 μM (AZnM1, △), 1.3 μM (AZnM2, ▽), 3.5 μM (AZnE1, ▽), 0.46 μM (AZnE2, ■), 196 μM (AZnE2, ○) of free Zn^{2+} ions. b) Two-photon emission spectra of AZnM2 in MOPS buffer solution (30 mM, 100 mM KCl, 10 mM NTA, pH 7.3) in the presence of free Zn^{2+} ions (0–1.3 μM). c) One- (●) and two-photon (○) fluorescence titration curves for the complexation of AZnM2 with various concentrations (0–0.13 μM) of free Zn^{2+} ions. d) Hill plots for the complexation of AZnM2 with free Zn^{2+} ions (0–0.13 μM) measured by one- (●) and two-photon (○) processes. The excitation wavelengths for one- and two-photon processes were 365 and 780 nm, respectively.

The dissociation constants (K_d^{OP} and K_d^{TP}) of AZnM1–AZnN for the one- and two-photon processes were calculated from the fluorescence titration curves.[3,6a] For all compounds, the titration curves fitted well with a 1:1 binding model and the Hill plots were linear with a slope of 1.0 (Figure 2c,d and the Supporting Information, Figure S1), thus indicating a 1:1 complexation between the probes and the Zn^{2+} ions.[13] The K_d^{OP} and K_d^{TP} values, which were almost the same within experimental errors, were in the range of 8.4 nM-12 μM (Table 1). The K_d values were always smaller for compounds with the MeO group (AZn1 > AZn2, AZnM1 > AZnM2, AZnE1 > AZnE2), which is in agreement with its capability of inducing a tighter binding (see above). Combined with AZn1 (K_d^{TP} = 1.1 nM) and AZn2 (K_d^{TP} = 0.5 nM), we now have a series of TP probes (AZn1–AZnN) with a wide range of binding affinities. We also measured the dissociation constant (K_d^i) in ionophore-treated HeLa cells by TPM (see the Supporting Information, Figure S2).[14] These K_d^i values were within experimental error of the values measured in MOPS buffer solution (Figure 1b), thus indicating that MOPS buffer solution represents the cytosolic environment reasonably well. Moreover, these values could be applied to the quantitative measurement of $[Zn^{2+}]_i$ ions by using $[Zn^{2+}]_i = K_d^i \cdot [(F-F_{min})/(F_{max}-F)]$, where F_{min}, F_{max}, and F are the two-photon excited fluorescence (TPEF) intensities in the absence and presence of excess Zn^{2+} ions and the observed TPEF intensity, respectively.[15]

AZn1–AZnE2 showed negligible response to Na^+, Ca^{2+}, and Mg^{2+} ions at 5 mM, and to Mn^{2+}, Fe^{2+}, Co^{2+}, Ni^{2+}, Cu^{2+}, and Cd^{2+} ions at 300 μM concentration. AZnN showed similar selectivity except that it had an appreciable response for Cd^{2+} ions (Figure 3). As Cd^{2+} ions are rarely present in biological systems, AZn1–AZnN can detect Zn^{2+} ions over a wide range of concentration without interference from other biologically relevant metal ions.

The fluorescence intensities of AZnM1–AZnN were pH insensitive over the range of pH 3.5–8.0. In the presence of excess Zn^{2+} ions, the fluorescence intensity of AZn-

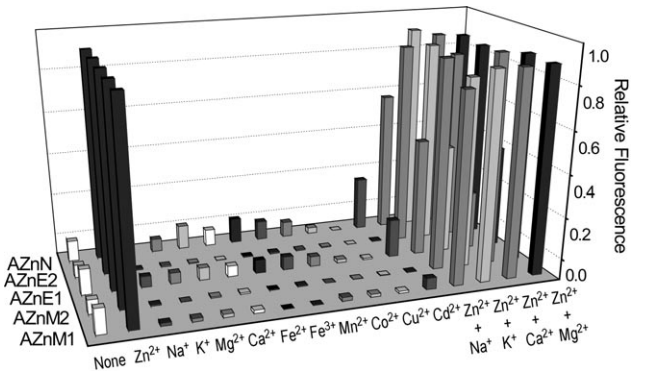

Figure 3. The relative fluorescence intensity of 1 μM AZnM1–AZnN in MOPS buffer solution (30 mM, 100 mM KCl, 10 mM NTA, pH 7.3) in the presence of 5 mM Na^+, K^+, Ca^{2+}, or Mg^{2+} ions, or 300 μM of Fe^{2+}, Fe^{3+}, Mn^{2+}, Co^{2+}, Cu^{2+}, or Cd^{2+} ions. Zn^{2+} ions were added at either 1 μM (AZnM1, AZnM2, AZnE2) or 3 μM (AZnE1) or 200 μM (AZnN). The data at $[Zn^{2+}]$ = 0 μM were determined in the presence of 10 mM NTA. The excitation wavelength was 365 nm.

CHEMISTRY
AN ASIAN JOURNAL

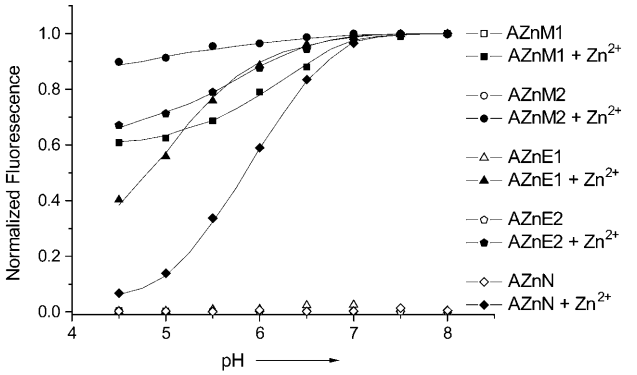

Figure 4. The effect of the pH value on the one-photon fluorescence intensity of 1 μM AZnM1–AZnN in the absence (open symbols) and presence of (closed symbols) excess Zn^{2+} ions in 30 mM MOPS buffer solution and 100 mM KCl at pH 7.3. The data at $[Zn^{2+}]=0$ μM were determined by adding 10 mM NTA. The excitation wavelength was 365 nm. The line is a guide to the eye.

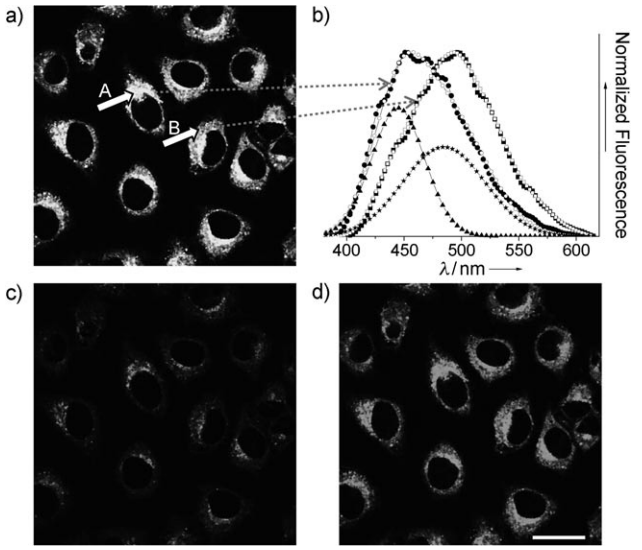

Figure 5. TPM images of AZnM2-labeled (2 μM) HeLa cells collected at 360–620 nm (a), 360–460 nm (c), and 520–620 nm (d). b) Two-photon-excited fluorescence spectra from the intense spot (A) and homogeneous domain (B) shown in (a), while the closed circle (●) and open square (□) correspond to the Gaussian functions fitted to the emission spectra. The triangle (▲) and star (★) represent the two Gaussian functions fitted to the black circle. The excitation wavelength was 780 nm. Cells shown are representative images from replicate experiments. Scale bar, 30 μm.

M1–AZnN remained nearly the same at pH > 7.0, and decreased at lower pH values (Figure 4). The decrease was appreciable for AZnE1 and significant for AZnN with the largest K_d value. This result can be attributed to the competing pathways for protonation and chelation of Zn^{2+} ions by the receptor moieties. Protonation would be the more-favorable event for a lower affinity probe at a lower pH value and would reduce the effective concentration of the probe–Zn^{2+} complex, thereby decreasing the fluorescence intensity. Nevertheless, the fluorescence intensity of the Zn^{2+} complexes with AZnM1–AZnN are not subject to interference by pH changes under near-neutral or slightly acidic conditions.

The TP cross-sections of the probe–Zn^{2+} complexes in MOPS buffer solutions were determined by a femtosecond (fs) fluorescence measurement technique, as reported previously.[16] The TP action spectra of the complexes indicated Φδ values of 86–110 GM (1 GM = 10^{-50} cm^4 s photon^{-1}) at 780 nm, values which exceeded those of TSQ and FluoZin-3 by 4~24-fold (Figure 2a and Table 1).[9] Thus, TPM images of the cells stained with AZn1–AZnN would be much brighter than those stained with the commercial probes.

Photostability was determined under the imaging conditions by monitoring the time-dependent decrease in the TP-excited fluorescence (TPEF) intensity in HeLa cells labeled with AZnM2 and AZnE1; measurements were made in four individual cells chosen without bias.[11d,f] The TPEF intensity decreased by approximately 5% within 1000 s and remained nearly the same for approximately 1 hour (see the Supporting Information, Figure S3). Similar results were observed for the other probes (data not shown). These studies showed that AZn1–AZnN has a high photostability and they are therefore suitable for long-term imaging applications.

The TPM image of the HeLa cells labeled with AZnM2 revealed intense spots (A) and homogeneous domains (B; Figure 5a). The homogeneous domain (B) could be fitted to a single Gaussian function (□) with an emission maximum at 495 nm, whereas the intense spot (A) could be fitted to two Gaussian functions with emission maxima at 445 (▲) and 485 nm (★; Figure 5b). The longer-wavelength bands (□ and ★) were similar to the emission spectrum of AZnM2 in the MOPS buffer solution, whilst the shorter-wavelength band (▲) was significantly blue-shifted. The differences in emission maxima suggest that the probes may be located in two regions of different polarity: a more-polar environment that is likely to be cytosol and a less-polar one that is likely to be membrane. Moreover, the shorter wavelength band (▲) decreased to the baseline at wavelength of < 520 nm. Consistently, the TPM image collected at 520–620 nm is homogeneous without intense spots (Figure 5d), whereas that collected at 360–460 nm clearly shows them (Figure 5c). Therefore, by using the detection window of 520–620 nm, we have detected cytosolic Zn^{2+} ions. We note that environmental sensitivity of these probes is beneficial to TPM where the detection window can be selected, whereas in fluorescence microscopy without a selective detection window, it may cause problems.

To demonstrate the utility of these probes, we have detected Zn^{2+} ions in the cultured HeLa cells by TPM. Earlier, we reported a bright TPM image of 293 cells labeled with AZn2 (K_d = 0.5 nM).[9] In contrast, the TPM images of HeLa cells labeled with AZnM2 (K_d = 8.4 nM) and AZnE1 (K_d = 480 nM) are dim (Figure 6a,b), presumably owing to their lower affinities for Zn^{2+} ions. When the cells were treated with Zn^{2+} ions and pyrithione (2-mercaptopyridine *N*-oxide, which can bring Zn^{2+} ions into the cytoplasm),[17] the TPEF intensity increased immediately. The increase was

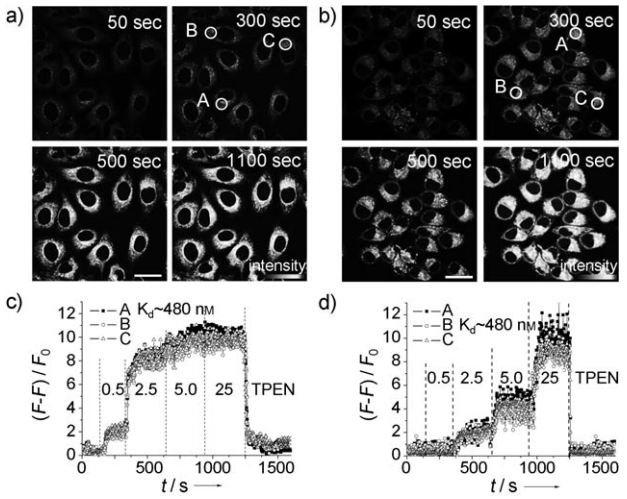

Figure 6. TPM images of HeLa cells incubated with a) AZnM2 and b) AZnE1 (2 μM) for 20 min at 37 °C. (c, d) Time courses of TPEF in individual cells as designated by the ○ for c) sample AZnM2 (from (a)) and d) sample AZnE1 (from (b)) after treatment with pyrithione/Zn^{2+} (1.0:0.5, 5.0:2.5, 5.0:5.0, 25:25 μM) and then with TPEN (0.1 mM) at intervals of 5 min. Images were collected at 520-620 nm with 1.6 s intervals using an excitation wavelength at 780 nm. Scale bar, 30 μm.

qualitatively proportional to the concentration of added Zn^{2+} ions, reaching the maximum concentration after the addition of 5.0 and 25 μM for the cells labeled with AZnM2 and AZnE1, respectively (Figure 6c,d). Also, the fluorescence intensity decreased abruptly to the baseline level upon addition of 0.1 mM *N,N,N′,N′*-terakis(2-pyridyl)ethylenediamine (TPEN), a membrane-permeable Zn^{2+} ion chelator that can effectively remove Zn^{2+} ions (Figure 6c,d).[6,7] Thus, the response time is very short and the TPEF is owing to the presence of probe–Zn^{2+} complexes in the cells.

To further assess the utility of these probes, we have detected Zn^{2+} ions deep inside live tissues. The bright field image of a part of fresh hippocampal slices from the postnatal 2-week-old rat incubated with 20 mM AZnM2–AZnN for 1 hour at 37 °C showed the CA1 and CA3 regions as well as the dentate gyrus (DG); the TPM images revealed the Zn^{2+} ion distribution in the same regions at a depth of 110 μm (see the Supporting Information, Figure S4). The TPM images of the slice labeled with AZnM2 showed intense fluorescence in the stratum lucidum (SL) of the CA3 region (Figure 7a). The image taken at a higher magnification clearly reveals the Zn^{2+} ion distribution in the same region (Figure 7b). The increase in the TPEF intensity after the addition of 50 mM KCl (Figure 7c,g) as a membrane depolarizer causing the release of Zn^{2+} ions, and the decrease in the TPEF upon treatment with TPEN (Figure 7d,h), provide supporting evidences for this observation.[18] When the tissue was labeled with AZnE2, the image was dim except in the SL where Zn^{2+} ions were more-concentrated, as predicted from the lower affinity (Figure 7a,e). Consistently, the TPM images of the tissue slices labeled with lower affinity probes became progressively dimmer (see the Supporting Information, Figure S4). Notably, the lower affinity probes

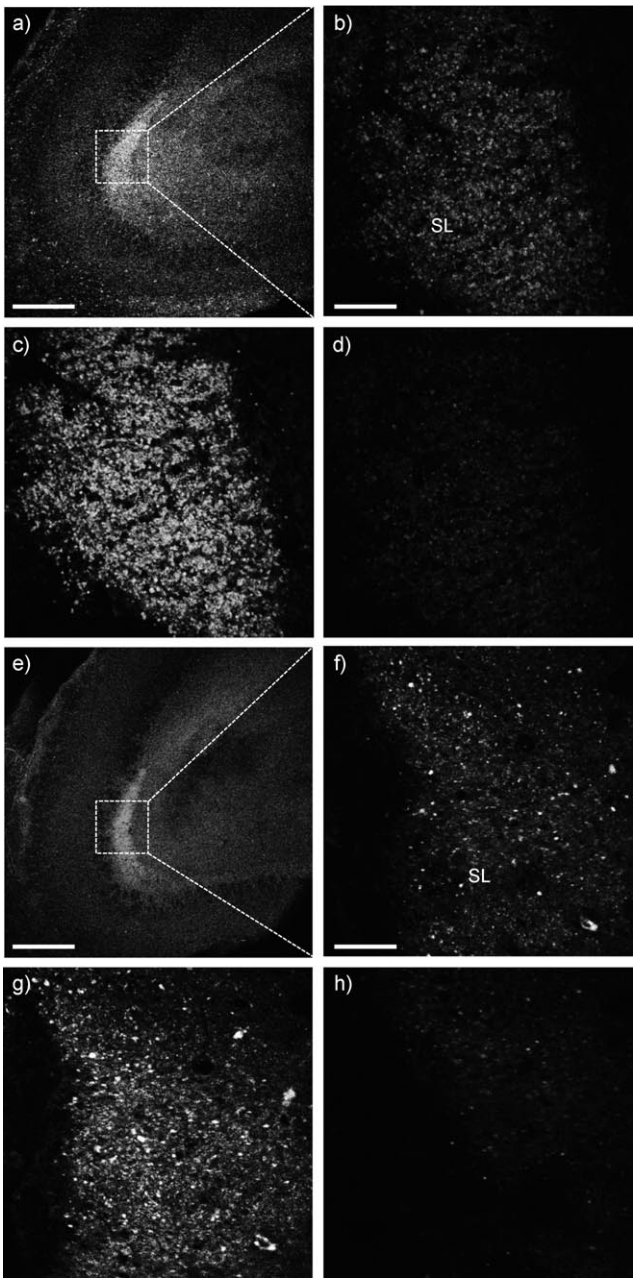

Figure 7. TPM images of slices of rat hippocampal labeled with 20 μM AZnM2 (a–d) and AZnE2 (e–h), respectively, for 1 h at 37 °C. a, e) TPM images at a depth of approximately 110 μm with magnification ×10. Scale bar, 300 μm. b–d, f–h) Magnification at ×100 in stratum lucidum (SL) of CA3 regions (white box) at a depth of approximately 120 μm before (b, f) and after addition of 50 mM KCl (c, g) to the imaging solution. d, h) After addition of 200 μM TPEN to (c) and (g), respectively. Scale bar, 30 μm. All images were collected at 520–620 nm and the excitation wavelength was 780 nm with fs pulses.

can highlight the Zn^{2+}-rich regions. Moreover, the TPM images of the slices labeled with AZnM2 revealed the Zn^{2+} ion distribution in the given *xy* plane of the CA3 region at 80–170 μm depth, thus indicating the sectioning capability of TPM (see the Supporting Information, Figure S5). These results demonstrate the capacity of AZnM1–AZnN to detect

Zn^{2+} ions over a wide range of concentrations in live tissues.

Conclusions

In conclusion, we have developed a series of TP Zn^{2+} probes (AZnM1-AZnN) with various K_d values ranging from sub-nanomolar to sub-millimolar. They show appreciable water solubility, cell permeability, significant TP action cross-sections when complexed with Zn^{2+} ions, high selectivity for Zn^{2+} ions, high photostability, pH insensitivity at pH > 7, and short response times. By using AZnM2 and AZnE1, different responses to changes in extracelluar Zn^{2+} ion concentration were observed. Moreover, the distribution of Zn^{2+} ions in the living rat-brain hippocampal slices could be detected by TPM at a depth of > 80 μm by using AZnM1–AZnN. Combined with the existing TP probes for Zn^{2+} ions (AZn1 and AZn2), AZn1–AZnN will find useful applications in the detection of various amounts of Zn^{2+} ions in live cells and intact tissues.

Experimental Section

Spectroscopic Measurements

Absorption spectra were recorded on a Hewlett–Packard 8453 diode array spectrophotometer, and fluorescence spectra were obtained with Aminco-Bowman series 2 luminescence spectrometer with a 1-cm standard quartz cell. The fluorescence quantum yield was determined with Coumarin 307 as the reference using a literature method.[18]

Water Solubility

A small amount of dye was dissolved in *N*,*N*-dimethylsulfoxide to prepare the stock solutions (1.0×10^{-3} M). The solution was diluted to (6.0×10^{-3} ~ 6.0×10^{-5} M) and added to a cuvette containing 3.0 mL of H_2O using a microsyringe. In all cases, the concentration of DMSO in H_2O was maintained at 0.2%.[19] The plots of fluorescence intensity against the dye concentration were linear at low concentration and showed downward curvature at higher concentrations. The maximum concentration in the linear region was taken as the solubility. The water solubilities of AZnM1–AZnN were in the range of 3.0–5.0 μM (AZnM1, 5.0 μM; AZnM2, 4.0 μM; AZnE1, 3.0 μM; AZnE2, 5.0 μM; AZnN, 4.0 μM).

Determination of Apparent Dissociation Constants

A series of MOPS (4-morpholinepropanesulfonic acid) buffer solutions (30 mM, pH 7.3, 0.1 M KCl) containing various amounts of $ZnSO_4$ (0~9.9 mM) and 10 mM of NTA (nitrilotriacetic acid) were prepared. The $[Zn^{2+}]_{free}$ was calculated from the K^{app}_{Zn-NTA}, $[NTA]_{total}$, and $[Zn^{2+}]_{total}$ by using Equation (1).[3, 20]

$$[Zn^{2+}]_{free} = [Zn^{2+}]_{total}/(\alpha_{Zn} \times K^{app}_{Zn-NTA} \times [NTA]_{free}) \quad (1)$$

Where,

$K^{app}_{Zn-NTA} = K_{Zn-NTA}/\alpha_{Zn}\alpha_{NTA}$,

$\alpha\alpha_{Zn} = 1 + 10^{(pH-pK_1)} + 10^{(2pH-pK_1-pK_2)} + 10^{(3pH-pK_1-pK_2-pK_3)}\ldots$

$\alpha\alpha_{NTA} = 1 + 10^{(pK_1-pH+0.11)} + 10^{(pK_1+pK_2-2pH+0.22)} + 10^{(pK_1+pK_2+pK_3-3pH+0.33)}\ldots$

and

$[NTA]_{free} = [NTA]_{total} - [Zn^{2+}]_{total}$

Thus,

$K^{app}_{Zn-NTA} = \frac{K_{Zn-NTA}(1+10^{(pK_{Zn-NTA}-pH)})}{(1+10^{(pH-pK_{Zn})})(1+10^{(pK_1-pH)}+10^{(pK_1+pK_2-2pH)})}$

Table 2. The calculated $[Zn^{2+}]$ free concentration of each solution.

$[Zn^{2+}]_{total}$ [mM]	1.0	2.0	3.0	4.0	5.0	5.5	6.0
$[Zn^{2+}]_{free}$ [nM]	0.85	1.9	3.3	5.1	7.6	9.2	11
$[Zn^{2+}]_{total}$ [mM]	6.9	7.1	8.0	8.4	9.0	9.4	9.9
$[Zn^{2+}]_{free}$ [nM]	17	19	30	41	65	130	1300

The stability constant for the Zn^{2+} complex of NTA (K_{Zn-NTA}) was taken from Ref. [22].

Thus, for NTA (pH 7.3, 0.1 M KCl, 25 °C), $pK_1 = 9.73$, $pK_2 = 2.49$, $pK_3 = 1.89$, log $K_{Zn-NTA} = 10.66$. All protonation constants must be corrected upward by 0.11 when determined in 0.1 M ionic-strength solutions. $[NTA]_{total}$ was set at 10 mM, and $[Zn^{2+}]_{total}$ was varied from 0–9.9 mM.

The calculated $[Zn^{2+}]_{free}$ concentration of each solution is shown in Table 2.

When $[Zn^{2+}]_{total}$ was over 9.9 mM in the NTA buffer system, various aliquots of 1–10 mM aqueous $ZnSO_4$ solutions were directly added to 30 mM MOPS buffer solution (0.1 M KCl, pH 7.3), which was treated with Chelex resin (Bio-Rad, manufacturer protocol).

To determine the apparent dissociation constants for the Zn^{2+} complex of probes, the fluorescence titration curves (Figure 1b) were obtained and fitted to Equation (2) (see Figure 2c).[6a, 22]

$$F = F_0 + (F_{max} - F_0)\frac{[Zn^{2+}]_{free}}{K_d + [Zn^{2+}]_{free}} \quad (2)$$

As shown in Equation (2), F is the fluorescence intensity, F_{max} is the maximum fluorescence intensity, F_0 is the fluorescence intensity in the absence of Zn^{2+} ions, and $[Zn^{2+}]_{free}$ is the free-Zn^{2+}-ion concentration. The K_d value that best fits the titration curve (Figure 2c) with Equation (2) was calculated by using the Excel program.

To determine the K_d^{TP} for the two-photon process, the TPEF spectra were obtained with a DM IRE2 Microscope (Leica) by using the *xyλ* mode at a scan speed of 800 Hz. The samples were excited by a mode-locked titanium-sapphire laser source (Coherent Chameleon, 90 MHz, 200 fs) set at a wavelength of 780 nm and an output power of 1180 mW, which corresponded to an average power in the focal plane of approximately 10 mW. The TPEF titration curves (Figure 2b) were obtained and fitted to Equation (2), as shown in Figure 2c.

Measurement of Two-Photon Cross-Sections

The two-photon cross-section (δ) was determined by using a femtosecond (fs) fluorescence measurement technique, as described before.[16] The probes were dissolved in 30 mM MOPS buffer solution (100 mM KCl, pH 7.3) at concentrations of 5.0×10^{-6} M and then the TPEF intensity was measured at 740–940 nm by using fluorescein (8.0×10^{-5} M, pH 11) as the reference, whose two-photon property has been well-characterized in the literature.[23] The emission intensities of the TPEF spectra of the reference and the sample were determined at the same excitation wavelength. The two-photon absorption (TPA) cross-section was calculated by using $\delta = \delta_r(S_s\Phi_r\varphi_r c_r)/(S_r\Phi_s\varphi_s c_s)$ where the subscripts s and r stand for the sample and reference molecules. The intensity of the signal collected by a CCD detector was denoted as S, the fluorescence quantum yield as Φ, and the overall fluorescence collection efficiency of the experimental apparatus as φ. The number density of the molecules in solution was denoted as c, whilst δ_r represents the TPA cross-section of the reference molecule.

Cell Culture and Imaging

HeLa human cervical carcinoma cells (ATCC, Manassas, VA, USA) were cultured in DMEM (WelGene Inc, Seoul, Korea) supplemented with heat-inactivated 10% FBS (WelGene Inc, Seoul, Korea), penicillin (100 units mL^{-1}), and streptomycin (100 μg mL^{-1}) at 37 °C in an incubator with a humidified atmosphere of 5% CO_2 and 95%. Three days before imaging, the cells were detached and were replaced on glass-bottomed dishes (MatTek). For labeling, the cells were rinsed with phosphate-buffered saline solution (DPBS; WelGene Inc) and incubated with 2 μM of

probe for 20 min at 37 °C. After washing with DPBS three times, the cells were mounted on the microscope stage and following addition of the indicated concentrations of $ZnSO_4$/pyrithione, they were imaged.

Two-Photon Fluorescence Microscopy

TPM images of the probe-labeled HeLa cell and tissues were obtained with spectral confocal and multiphoton microscopes (Leica TCS SP2) with ×100 oil and ×10 dry objective, numerical aperture (NA) = 1.30 and 0.3, respectively. The TPM images were obtained with a DM IRE2 Microscope (Leica) by exciting the probes with a mode-locked titanium-sapphire laser source (Coherent Chameleon, 90 MHz, 200 fs) set at wavelength 780 nm and output power 1180 mW, which corresponded to approximately 10 mW average power in the focal plane. To obtain images at the 360~620 nm, 360~460 nm, and 500~620 nm ranges, internal PMTs were used to collect the signals in an 8 bit unsigned 512×512 pixels at 400 Hz scan speed.

Preparation and Staining of Fresh Rat-Hippocampal Slices

All experiments were performed in accordance with the guidelines established by the Committee of Animal Research Policy of Korea University College of Medicine. Rats that were 2 weeks old were sacrificed by cervical dislocation within 2 hours of arrival. Slices were prepared from the hippocampi of 2-week-old rats (SD). Coronal slices (400 μm thick) were cut by using a vibrating-blade microtome in artificial cerebrospinal fluid (ACSF; 124 mM NaCl, 3 mM KCl, 26 mM $NaHCO_3$, 1.25 mM NaH_2PO_4, 10 mM D-glucose, 2.4 mM $CaCl_2$, and 1.3 mM $MgSO_4$). Slices were incubated with 20 mM of the probes in ACSF bubbled with 95% O_2 and 5% CO_2 for 1 hour at 37 °C. Slices were then washed three times with ACSF and transferred to glass-bottomed dishes (MatTek) and observed by using a spectral confocal multiphoton microscope.

Acknowledgements

This work was supported by a National Research Foundation (NRF) grant funded by the Korean Government (No. 2010-0018921), and by a Priority Research Centers Program through the NRF funded by the Ministry of Education, Science and Technology (No. 2010-0020209). I.A.D., C.S.L., J.H.H., and M.Y.K. were supported by a BK21 scholarship.

[1] a) B. L. Vallee, K. H. Falchuk, *Physiol. Rev.* **1993**, *73*, 79–118; b) J. M. Berg, Y. G. Shi, *Science* **1996**, *271*, 1081–1085.
[2] a) C. J. Frederickson, J.-H. Koh, A. I. Bush, *Nat. Neurosci.* **2005**, *6*, 449–462; b) S. Y. Assaf, S. H. Chung, *Nature* **1984**, *308*, 734–736; c) G. A. Howell, M. G. Welch, C. J. Frederickson, *Nature* **1984**, *308*, 736–738.
[3] C. J. Fahrni, T. V. O'Halloran, *J. Am. Chem. Soc.* **1999**, *121*, 11448–11458.
[4] K. Kikuchi, K. Komatsu, T. Nagano, *Curr. Opin. Chem. Biol.* **2004**, *8*, 182–191.
[5] D. W. Domaille, E. L. Que, C. J. Chang, *Nat. Chem. Biol.* **2008**, *4*, 168–175.
[6] a) T. Hirano, K. Y. Urano, T. Nagano, *J. Am. Chem. Soc.* **2002**, *124*, 6555–6562; b) K. Komatsu, K. Kikuchi, H. Kojima, Y. Urano, T. Nagano, *J. Am. Chem. Soc.* **2005**, *127*, 10197–10204; c) K. Komatsu, Y. Urano, H. Kojima, T. Nagano, *J. Am. Chem. Soc.* **2007**, *129*, 13447–13454.
[7] a) S. C. Burdette, C. J. Frederickson, W. Bu, S. J. Lippard, *J. Am. Chem. Soc.* **2003**, *125*, 1778–1787; b) C. J. Chang, J. Jaworski, E. M. Nolan, M. Sheng, S. J. Lippard, *Proc. Natl. Acad. Sci. USA* **2004**, *101*, 1129–1134; c) E. M. Nolan, J. W. J. Jaworski, R. P Feazell, M. Sheng, S. J. Lippard, *J. Am. Chem. Soc.* **2006**, *128*, 15517–15528.
[8] a) R. M. Williams, W. R. Zipfel, W. W. Webb, *Curr. Opin. Chem. Biol.* **2001**, *5*, 603–608; b) W. R. Zipfel, R. M. Williams, W. W. Webb, *Nat. Biotechnol.* **2003**, *21*, 1369–1377; c) F. Helmchen, W. Denk, *Nat. Methods* **2005**, *2*, 932–940.
[9] H. M. Kim, M. S. Seo, M. J. An, J. H. Hong, Y. S. Tian, J. H. Choi, O. Kwon, K. J. Lee, B. R. Cho, *Angew. Chem.* **2008**, *120*, 5245–5248; *Angew. Chem. Int. Ed.* **2008**, *47*, 5167–5170.
[10] C. J. Frederickson, M. A. Klitenick, W. I. Manton, J. B. Kirkpatrick, *Brain Res.* **1983**, *273*, 335–339.
[11] a) H. M. Kim, B. R. Cho, *Acc. Chem. Res.* **2009**, *42*, 863–872; b) P. S. Mohan, C. S. Lim, Y. S. Tian, W. Y. Roh, J. H. Lee, B. R. Cho, *Chem. Commun.* **2009**, 5365–5367; c) Y. S. Tian, Lee, H. Y. , C. S. Lim, J. M. Park, H. M. Kim, Y. N. Shin, E. S. Kim, H. J. Jeon, S. B. Park, B. R. Cho, *Angew. Chem.* **2009**, *121*, 8171–8175; *Angew. Chem. Int. Ed.* **2009**, *48*, 8027–8031; d) M. K. Kim, C. S. Lim, J. T. Hong, J. H. Han, H. Y. Jang, H. M. Kim, B. R. Cho, *Angew. Chem.* **2010**, *122*, 374–377; *Angew. Chem. Int. Ed.* **2010**, *49*, 364–367; e) J. H. Lee, C. S. Lim, Y. S. Tian, J. H. Han, B. R. Cho, *J. Am. Chem. Soc.* **2010**, *132*, 1216–1217; f) C. S. Lim, D. W. Kang, Y. S. Tian, J. H. Han, H. L. Hwang, B. R. Cho, *Chem. Commun.* **2010**, *46*, 2388–2390.
[12] C. Reichardt, *Chem. Rev.* **1994**, *94*, 2319–2358.
[13] K. A. Connors, *Binding Constants*, Wiley, New York, **1987**.
[14] H. M. Kim, P. R. Yang, M. S. Seo, J.-S. Yi, J. H. Hong, S.-J. Jeon, Y.-G. Ko, K. J. Lee, B. R. Cho, *J. Org. Chem.* **2007**, *72*, 2088–2096.
[15] R. E. London, *Annu. Rev. Physiol.* **1991**, *53*, 241–258.
[16] S. K. Lee, W. J. Yang, J. J. Choi, C. H. Kim, S.-J. Jeon, B. R. Cho, *Org. Lett.* **2005**, *7*, 323–326.
[17] a) B. L. Barnett, H. C. Kretschmar, F. A. Hartman, *Inorg. Chem.* **1977**, *16*, 1834–1838; b) C. J. Chandler, I. H. Segel, *Antimicrob. Agents Chemother.* **1978**, *14*, 60–68.
[18] J. N. Demas, G. A. Crosby, *J. Phys. Chem.* **1971**, *75*, 991–1024.
[19] H. M. Kim, H.-J. Choo, S.-Y. Jung, Y.-G. Ko, W.-H. Park, S.-J. Jeon, C. H. Kim, T. Joo, B. R. Cho, *ChemBioChem* **2007**, *8*, 553–559.
[20] M. Taki, J. L. Wolford, T. V. O'Halloran, *J. Am. Chem. Soc.* **2004**, *126*, 712–713.
[21] A. E. Martell, R. M. Smith, NIST Critical Stability Constants of Metal Complexes. NIST Standard Reference Database 46, Version 7.0, 2003.
[22] T. Hirano, K. Kikuchi, Y. Urano, T. Higuchi, T. Nagano, *J. Am. Chem. Soc.* **2000**, *122*, 12399–12400.
[23] C. Xu, W. W. Webb, *J. Opt. Soc. Am. B* **1996**, *13*, 481–491.

Received: October 4, 2010
Published online: February 17, 2011

